

A time-varying inertia pendulum: Analytical modelling and experimental identification

*Original*

A time-varying inertia pendulum: Analytical modelling and experimental identification / Bellino, Andrea; Fasana, Alessandro; Gandino, Edoardo; Garibaldi, Luigi; Marchesiello, Stefano. - In: MECHANICAL SYSTEMS AND SIGNAL PROCESSING. - ISSN 0888-3270. - 47:(2014), pp. 120-138. [10.1016/j.ymssp.2013.03.012]

*Availability:*

This version is available at: 11583/2543097 since: 2016-03-01T15:23:43Z

*Publisher:*

Elsevier

*Published*

DOI:10.1016/j.ymssp.2013.03.012

*Terms of use:*

This article is made available under terms and conditions as specified in the corresponding bibliographic description in the repository

*Publisher copyright*

(Article begins on next page)

# A time-varying inertia pendulum: analytical modelling and experimental identification

A. Bellino, A. Fasana, E. Gandino, L. Garibaldi, S. Marchesiello<sup>\*</sup>

*Dipartimento di Ingegneria Meccanica e Aerospaziale, Politecnico di Torino*

*C.so Duca degli Abruzzi 24, 10129 Torino, Italy*

## **Abstract**

In this paper two of the main sources of non-stationary dynamics, namely the time-variability and the presence of nonlinearity, are analyzed through the analytical and experimental study of a time-varying inertia pendulum. The pendulum undergoes large swinging amplitudes, so that its equation of motion is definitely nonlinear, and hence becomes a nonlinear time-varying system. The analysis is carried out through two subspace-based techniques for the identification of both the linear time-varying system and the nonlinear system.

The flexural and the nonlinear swinging motions of the pendulum are uncoupled and are considered separately: for each of them an analytical model is built for comparisons and the identification procedures are developed. The results demonstrate that a good agreement

---

<sup>\*</sup> Corresponding author. Tel.: +390110906947; fax: +390110906999; e-mail address: stefano.marchesiello@polito.it

between the predicted and the identified frequencies can be achieved, for both the considered motions. In particular, the estimates of the swinging frequency are very accurate for the entire domain of possible configurations, in terms of swinging amplitude and mass position.

## **Keywords**

Pendulum; moving mass; nonlinear identification; time-varying analysis.

## **1. Introduction**

During the last years, many efforts have been spent in studying non-stationary signals.

Within this topic, two fundamental sources of non-stationarity are the time-variability and the presence of nonlinearity.

Classical examples of time-varying systems are absorber springs with non-constant stiffness, or fuel tanks, characterized by mass variation. Another important class of time-varying systems is the case of moving loads: if a structure is travelled by a load whose mass is not negligible with respect to the structure mass, then the dynamical properties of the system change with time. Typical case is a train crossing a railway bridge.

One of the first works on the identification of time-varying systems was conducted by Liu [1, 2], where the concept of pseudo-natural frequencies was introduced, that are obtained by the time-varying state transition matrix. Tasker [3] proposed a recursive algorithm, based on subspace methods, to identify the state matrices and successively to determine the modal parameters. Other important approaches are those based on the Kalman Filter [4], or the parametric methods, as for example the FS-TARMA [5], which is an extension of the classical ARMA techniques.

In [6], a Short-Time Stochastic Subspace Identification (ST-SSI) approach has been defined, based on the “frozen” technique, where the classical subspace identification [7] is applied to successively windowed parts of the signal.

The ST-SSI method can be applied to different kinds of non-stationary systems in order to estimate the instantaneous frequencies of the signal. For example, it has been used to estimate the frequency in nonlinear systems, as well as in practical systems showing nonlinear effects, such as pre-stressed concrete beams tested in laboratory, in which a softening nonlinearity was identified [8]. In a similar way, an input-output linear system subspace identification method has been applied in [9] for characterization of nonlinear dynamical structural systems: time-varying instantaneous natural frequencies and mode shapes of nonlinear civil structures are extracted.

However, instead of extracting a series of time-varying linear models, the identification of a whole parametric nonlinear model is an important instrument for many purposes. For example, it would allow for treating nonlinearities in possibly damaged structures [10], or attaining improved predictions of vibration response amplitude, which is an issue for accurate long term fatigue estimates. Any nonlinear method is requested to correctly identify the classes of nonlinearity present and possibly to quantify the extent of their force contributions. Nonlinear system identification has been thoroughly investigated in recent years and many efforts have been spent leading to a large number of methods. A comprehensive list describing the past and recent developments is given in [11].

Among them, the Conditioned Reverse Path (CRP) method [12, 13] is based on the construction of a hierarchy of uncorrelated response components in the frequency domain, allowing the estimation of the coefficients of the nonlinearities away from the location of

the applied excitation.

The Nonlinear Identification through Feedback of the Outputs (NIFO) [14] is a frequency domain method which has demonstrated some advantages with respect to the CRP, mainly due to the lighter conceptual and computing effort. This method exploits the spatial information and interprets nonlinear forces as unmeasured internal feedback forces.

Starting from the basic idea of NIFO, the Nonlinear Subspace Identification (NSI) method has been developed [15] and improved [16] for identifying large systems with lumped nonlinearities. NSI is a time domain method which exploits the robustness and the high numerical performances of the subspace algorithms. In order to extend the NSI method to be applied also on realistic large nonlinear engineering structures, a modal counterpart has been developed in [17].

In the present paper, both the ST-SSI and the NSI methods are applied to the experimental case of a pendulum with time-varying inertia. Moreover, a nonlinear behaviour is expected, since the swinging angles are large.

The analysis and simulation [18] of mechanical systems with imposed relative motion of components is challenging: time-varying inertia, created by a part that slides along a rotating member, reveals the Coriolis-type effects present in the system. This relative movement can excite but also reduce the structure vibration, providing new means or techniques for active attenuation of vibrations. An example of such a technique, in which a mass moving radially is treated as a controller to attenuate the pendulum swings, was demonstrated in [19].

The concept of controlling the motion of a system through mass reconfiguration has been examined in [20] using a variable length mathematical pendulum. The control of angular

oscillations is accomplished by sliding the end mass towards and away from the pivot. A variable length pendulum has also been considered in [21], where a rigorous qualitative investigation of its equation is carried out without any assumption on small swinging amplitudes. The exact and approximate study of the nonlinear pendulum can be found in various recent papers; most of them deal with obtaining analytical approximate expressions for the large-angle pendulum period [22, 23]. Among the few papers devoted to obtaining approximate solutions (the angular displacement as a function of time), [24] derives an accurate expression in terms of elementary functions.

The paper starts with an overview of the ST-SSI and the NSI methods; then, in Section 3, the experimental setup is described and the fundamental relationships about the dynamics of the pendulum are extracted. In Section 4, a model for the pendulum is proposed for the flexural vibrations and successively the identified frequencies are compared to those obtained by the Rayleigh-Ritz approach. In Section 5, the swing motion of the pendulum is considered, firstly with a fixed mass and then with a moving mass travelling on it. The final results show that the identified swinging frequency and the theoretical one are very similar.

## **2. Methodology**

Before discussing the experimental application, it is necessary to briefly introduce the identification methods that can be used in this particular case. To the authors' knowledge, there are no methodologies able to perform a reliable identification by taking the two effects into account, therefore an explanation of two methods, one specific for linear time-varying systems and one *ad hoc* for nonlinear systems, is proposed.

Both the presented procedures are based on the subspace methods introduced by Van Overschee and De Moor [7].

### 2.1. ST-SSI method

The procedure for the identification of linear time-varying systems is called Short-Time Stochastic Subspace Identification (ST-SSI) [6, 25]. The idea is to divide the signal in many parts and consider the system as time-invariant in each time interval: the process is called frozen technique.

If the output data are measured at discrete times with a sampling interval  $\Delta t$  and the input is a discrete signal characterised by a zero-order hold between consecutive sample points, the corresponding discrete-time state-space representation of a general linear time-varying system at a time instant  $t = r\Delta t$  is:

$$\begin{cases} x(r+1) = A(r)x(r) + B(r)u(r) + w(r) \\ y(r) = C(r)x(r) + D(r)u(r) + v(r) \end{cases} \quad (1)$$

where  $A(r)$  and  $B(r)$  are not constant and in general their closed forms are unknown [2];  $x(r)$  is the state vector,  $u(r)$  the input vector and  $y(r)$  the output vector;  $w(r)$  and  $v(r)$  are process error and measurement error, respectively.

The frozen technique considers the state matrices as constant during each time step so that

$$\begin{cases} x(r+1) = Ax(r) + Bu(r) + w(r) \\ y(r) = Cx(r) + Du(r) + v(r) \end{cases} \quad (2)$$

The complete time record is split into time windows (frozen system) almost completely overlapping except for a sampling period  $\tau$  (or its multiple).

The natural frequencies are extracted by calculating the eigenvalues of the identified matrix  $A$  in every window. The length of the window  $L_f$  is usually chosen as short as possible, in order to consider a brief time interval and hopefully a time-invariant system. This is the main reason why the data-driven approach [7] is preferred with respect to the covariance-driven one [26], which needs more samples to obtain accurate results.

For these reasons, the ST-SSI method can be used to analyse non-stationary systems that are regarded as time-invariant in each user-defined short time-interval, provided they change “slowly” with time. The term “slowly” here mainly means that their time variations are by far longer than their dynamics, i.e. the frequency ranges are well apart.

## 2.2. NSI method

The procedure for the identification of nonlinear systems is called Nonlinear Subspace Identification (NSI) [15]. A dynamical system with  $h$  degrees of freedom and with lumped nonlinear springs and dampers can be described by the following equation of motion:

$$M\ddot{z}(t) + C_v\dot{z}(t) + Kz(t) = f(t) - \sum_{j=1}^p \mu_j L_{nj} g_j(z, \dot{z}) = f(t) + f_{nl}(t) \quad (3)$$

where  $M$ ,  $C_v$  and  $K$  are the mass, viscous damping and stiffness matrices respectively,  $z(t)$  is the generalised displacement vector and  $f(t)$  the generalised force vector, both of dimension  $h$ , at time  $t$ . Each of the  $p$  nonlinear components depends on the scalar nonlinear function  $g_j(z, \dot{z}) = g_j(t)$ , which specifies the class of the nonlinearity (e.g., Coulomb friction, clearance, quadratic damping, etc.), and on a scalar coefficient  $\mu_j$ . The vector  $L_{nj}$ , whose entries may assume the values 1, -1 or 0, is related to the location of each nonlinear element.

According to Eq. (3), the original system may be regarded as subjected to the external forces  $f(t)$  and the internal feedback forces due to nonlinearities  $f_{nl}(t)$ , expressed as the sum of the  $p$  nonlinear components.

As shown in [15], matrices  $A$ ,  $B$ ,  $C$  and  $D$  of the discrete state-space model written in the same form as Eq. (2) can be defined from the equation of motion in Eq. (3). Observe



that the input vector is defined as  $u(r) = \begin{bmatrix} f(r)^T & -g_1(r) & K & -g_p(r) \end{bmatrix}^T$  and the information about nonlinearities is only contained in matrices  $B$  and  $D$ .

The nonlinear identification procedure is based on the computation of system parameters, once the state space matrices have been estimated by a subspace method [7] in the time domain. In fact, system parameters (included in  $M, C_v, K$  and  $\mu_j$ ) are contained in the matrix

$$H_E(\omega) = D + C(zI - A)^{-1}B, \quad z = \exp(j\omega\Delta t) \quad (4)$$

which is invariant under the similarity transformation corresponding to the application of a subspace method [15].

Without an applied force, a different type of analysis can be performed by considering the system as subject to initial conditions or impulsive excitation. This situation has been studied in [17] for SDOF systems and, in general, the exact nonlinear coefficients  $\mu_j$  cannot be obtained. However, in this particular case the system is a pendulum and its equation of motion allows some considerations about nonlinearity, which will be described in Section 5.

In general, if the force contribution due to nonlinearities is constant with respect to the linear one, the NSI method can be extended over the entire time history, without loss of effectiveness. In the present case, the lack of a forcing term leads the swinging amplitudes of the pendulum to decrease so that the contribution of nonlinearities (which are due to large amplitudes) is also decreasing. For this reason, the NSI method is applied over a certain number of windows in time. In particular, as shown in Section 5, the windows will be selected where the amplitudes are large, i.e. where the nonlinear contribution is

sufficiently high to be clearly identified.

### **3. Experimental set up**

The structure under testing is a pendulum with time-varying inertia: a disk on a cart can travel along it through a runner, while the pendulum is swinging. Moreover, this structure cannot be considered simply as a linear time-variant system, since for large swinging amplitudes the equation of motion of the pendulum has to be considered as nonlinear.



**Fig. 1.** Detail of the runner and the cart.



**Fig. 2.** Complete structure. At the top, the plate added to the system to enforce the clamp is highlighted. The travelling mass and the counterweight are observable on the left and on the right, respectively.

### *3.1. Description*

An overview of the design of the structure is presented in this section, together with a description of the instrumentation used for acquiring data. The measured characteristics of the considered elements, such as mass and dimensions, are defined in next section, where the equation of motion is introduced.

The pendulum is constituted by an aluminium runner along which a cart can slide, as represented in Fig. 1. The cart has two screw holes for mounting an added mass which can

slide on the pendulum, thus varying its inertia.

Moreover, in order to avoid a non optimal clamp between the runner and the shaft due to the large deformability of aluminium, a small plate has been added to the system to enforce the clamp.

The travelling mass is a steel disk, whose motion is regulated by a counterbalancing mass driven by hand without affecting the pendulum swing. This counterweight is connected to the moving mass through a system of pulleys and a cable that can be considered as non-extendable. The complete structure is shown in Fig. 2, with the sensors described in next section. The main supports, plates, pulleys, bearings and precision shaft are observable.

#### 3.1.1. Instrumentation

The sensors can be seen in Fig. 2. A triaxial and four monoaxial accelerometers have been mounted along the beam: information about their masses and positions is given in Table 1. Their characteristics will be useful for elaborating some considerations about the parameter updating that is performed in Section 5.1.

The triaxial accelerometer is a PCB 356B18 piezoelectric sensor (ICP). It has not been used for the analyses presented in this paper but its mass has to be considered in Section 5.1, since the sensor was included in the setup during all measurements.

Each monoaxial accelerometer is a Brüel&Kjær 4507 B 004 piezoelectric sensor. These sensors are used to measure the transversal vibrations of the pendulum, for performing the ST-SSI analysis of Section 4.

A direct measure of the angular position of the pendulum is given by a Penny+Giles SRS280 sealed rotary sensor, with an accuracy of  $\pm 1\%$  over  $100^\circ$ , connected to the precision shaft.

A Celesco PT1A linear potentiometer, with a maximum extension of 1.2 m, has been connected to the counterweight (see Fig. 2). The position of the travelling mass along the runner can be simply obtained from this measure.

All signals have been acquired with a sampling frequency of 256 Hz. The signals have been measured by using an OROS acquisition system, with 32 channels and anti-aliasing filter.

**Table 1**  
Characteristics of the accelerometers.

Type	Mass	Distance from the pivot point
Monoaxial	$m_{mono} = 0.0046 \text{ kg}$	$s_{mono,1} = 0.205 \text{ m}$
		$s_{mono,2} = 0.525 \text{ m}$
		$s_{mono,3} = 0.750 \text{ m}$
		$s_{mono,4} = 0.980 \text{ m}$
Triaxial	$m_{tri} = 0.0243 \text{ kg}$	$s_{tri} = 0.930 \text{ m}$

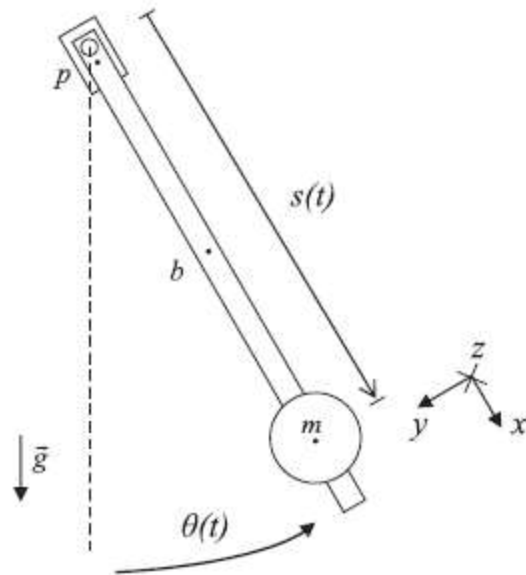


**Fig. 3.** Pendulum with the travelling mass.

### 3.2. Equation of motion

In this section, the pendulum with a travelling mass is considered as vibrating in two directions: in the flexural direction (the  $z$  axis in Fig. 3) the system behaves as a linear continuous beam, while in the orthogonal direction  $y$  the swinging pendulum can be

considered as a simple nonlinear SDOF system, since the flexural stiffness along this direction is very high. In the following, these two motions will be referred to as “flexural” and “swinging” motion respectively.

Note that the two motions can be considered as uncoupled: flexural vibrations are influenced by the effect of an axial force (tensile positive) due to gravity. For the beam of this experimental application the contribution of gravity, which depends on  $\theta(t)$  (Fig. 3), can be considered as negligible on the basis of results in [27].

From the rotational equilibrium of the system shown in Fig. 3, the equation of the “swinging” motion can be derived as follows:

$$(I_{p0} + I_{b0} + I_{m0}(t))\ddot{\theta}(t) + (c_v + 2m_m s(t)\dot{s}(t))\dot{\theta}(t) + (m_p g d_p + m_b g d_b + m_m g s(t))\sin\theta(t) = I_{tot}(t)\ddot{\theta}(t) + C_{tot}(t)\dot{\theta}(t) + P_{tot}(t)\sin\theta(t) = 0 \quad (5)$$

in which the subscripts  $p$ ,  $b$  and  $m$  refer to the plate, the beam and the travelling mass, respectively. The angle swept by the pendulum is indicated by  $\theta(t)$ . Other terms appearing in Eq. (5) are the position  $s(t)$  of the travelling mass, the acceleration of gravity  $g = 9.81 \text{ m/s}^2$  and a viscous damping coefficient  $c_v$ .

For each component of the system, the properties have been measured and are reported in Table 2; their moments of inertia have been computed with respect to the pivot point  $O$  as follows:

$$I_{p0} = \frac{1}{12} m_p (a_p^2 + b_p^2) + m_p d_p^2 \quad (6a)$$

$$I_{b0} = \frac{1}{12} m_b L_b^2 + m_b d_b^2 \quad (6b)$$

$$I_{m0} = \frac{1}{2} m_m r_m^2 + m_m s(t)^2 = I_m + m_m s(t)^2 \quad (6c)$$

When the travelling mass is fixed on the beam, then  $s(t) = \bar{s}$ ,  $\dot{s}(t)=0$  and the following restricted forms of Eq. (5) are considered:

$$\begin{aligned}
& (I_{p0} + I_{b0} + I_{m0})\ddot{\theta}(t) + c_v\dot{\theta}(t) + (m_pg d_p + m_bg d_b + m_m g \bar{s})\sin\theta(t) \\
& = (I + m_m \bar{s}^2)\ddot{\theta}(t) + c_v\dot{\theta}(t) + (P + m_m g \bar{s})\sin\theta(t) \\
& = \bar{I}_{tot}\ddot{\theta}(t) + c_v\dot{\theta}(t) + \bar{P}_{tot}\sin\theta(t) = 0
\end{aligned} \tag{7}$$

where  $I = I_{p0} + I_{b0} + I_m$  and  $P = m_pg d_p + m_bg d_b$ .

**Table 2.** Characteristics of the components.

Component	Mass (kg)	Sizes (m)	Centre of mass distance from $O$ (m)
Plate	0.0713	$a_p = 0.044$ , $b_p = 0.063$	$d_p = 0.01$
Beam	0.29	$L_b = 1$	$d_b = 0.5$
Travelling Mass	0.5025	$r_m = 0.05$	$s(t)$

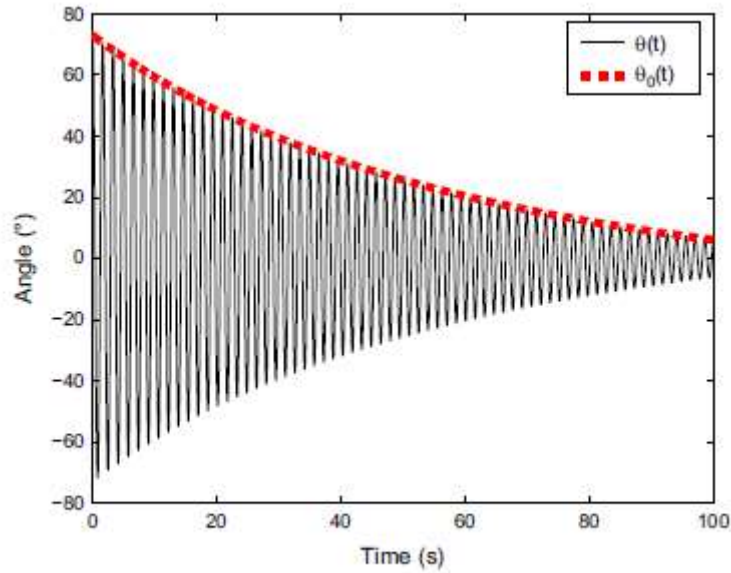


**Fig. 4.** Representation of the angle  $\theta(t)$  and the maximum amplitude  $\theta_0(t)$ .

### 3.2.1. Swinging frequency

When the swings are not “small”, i.e. the linearization  $\sin \theta \cong \theta$  of Eq. (5) is not possible, the swinging period of the pendulum depends on its angular amplitude. An analytical expression of the swinging frequency of the undamped pendulum is:

$$\bar{f} = f(\bar{s}) = \frac{\pi}{2} \frac{1}{T_0(\bar{s})K(k)}, \quad (8)$$

where  $T_0$  is the period for “small” swings and  $K(k)$  is the incomplete elliptic integral of the first kind. The complete procedure for deriving Eq. (8) is described in Appendix A.

In order to derive an analytical representation of frequency for large swings in presence of small damping, in this paper we simply extend Eq. (8) by considering the swinging frequency as “instantaneous”: for each value of time  $t$  the pendulum is seen as a new system having a new maximum amplitude  $\theta_0$ , which implies a new value of  $K(k)$  and consequently a new value of  $\bar{f}(t)$  in Eq. (8).

The meaning of  $\theta_0(t)$  is shown in Fig. 4: it can be seen as a time-varying maximum amplitude. Note that  $\theta_0(t)$  can be computed (for example, by interpolation of maxima/minima) only *a posteriori*, after having full knowledge of the time history of  $\theta(t)$ .

Then, the new definition of frequency is given as follows:

$$\bar{f}(t) = f(\bar{s}, \theta_0(t)) = \frac{\pi}{2} \frac{1}{T_0(\bar{s})K(k(t))}, \quad (9)$$

where  $k(t) = \sin(\theta_0(t)/2)$ .

A nonlinear effect can then be observed in Eq. (9): the large swings of the pendulum affect the elliptic integral  $K(k(t))$ . Moreover, this nonlinear contribution is decreasing in time, since the maximum amplitude is reduced by damping, and the frequency tends to the value



$f_0 = 1/T_0(\bar{s})$  assumed for small swings. An example of this latter effect is given in Fig. 5, where Eq. (9) is used to compute the frequency for the mass in a fixed position  $\bar{s} = 0.5$  m.

### 3.2.2. Baseline frequencies for fixed mass positions

Eq. (9) is useful as an analytical “expectation” that can be adopted for comparisons with the identified results of Section 5. In particular, in order to analyse the cases with the travelling mass, a representation of some curves, for fixed values of  $\bar{s}$ , can be used as a baseline grid. This is shown in Fig. 6, in which the frequencies are plotted as a function of the maximum amplitude of swing, for 10 equally spaced mass positions  $\bar{s}$ . It can be observed that the 10 curves have the same behaviour, as expected. Moreover, if a fixed value of  $\bar{\theta}_0$  is considered, the frequencies are not monotonic with the position  $\bar{s}$ . In fact, they are increasing for values of  $\bar{s}$  between 0.95 m and 0.25 m, but then they start decreasing for  $\bar{s} = 0.15$  m and 0.05 m. This is due to the values assumed by the characteristics of the components (Table 2) and is confirmed by showing in Fig. 7 the behaviour of the small-swings frequency  $f_0$  as a function of  $\bar{s}$ :

$$f_0(\bar{s}) = \frac{1}{2\pi} \sqrt{\frac{P + m_m g \bar{s}}{I + m_m \bar{s}^2}}. \quad (10)$$

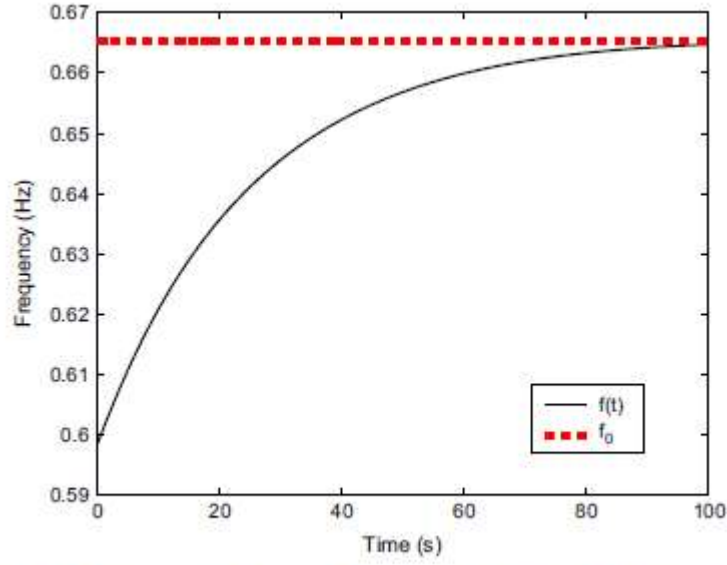


**Fig. 5.** Example of swinging frequency, with the mass in a fixed position  $\bar{s}=0.5$  m.

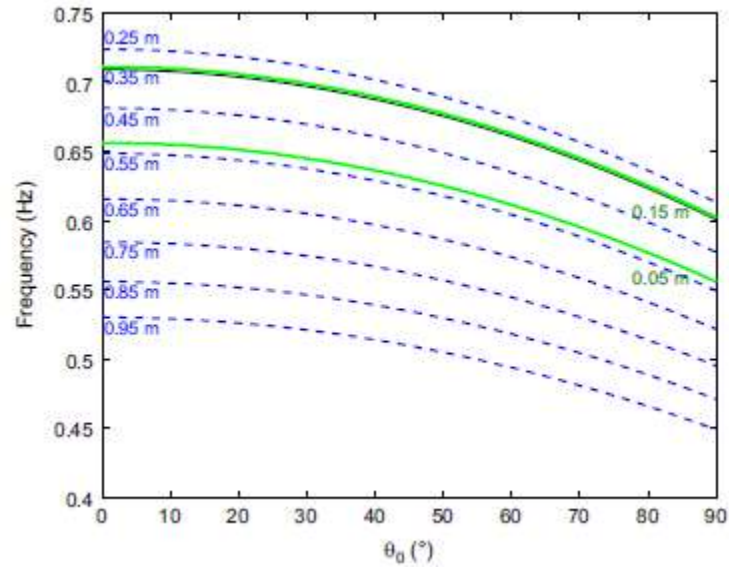


**Fig. 6.** Representation of the time-varying frequencies as a function of the maximum amplitude  $\theta_0(t)$ , for different fixed mass positions  $\bar{s}$  (indicated in meters on the figure).

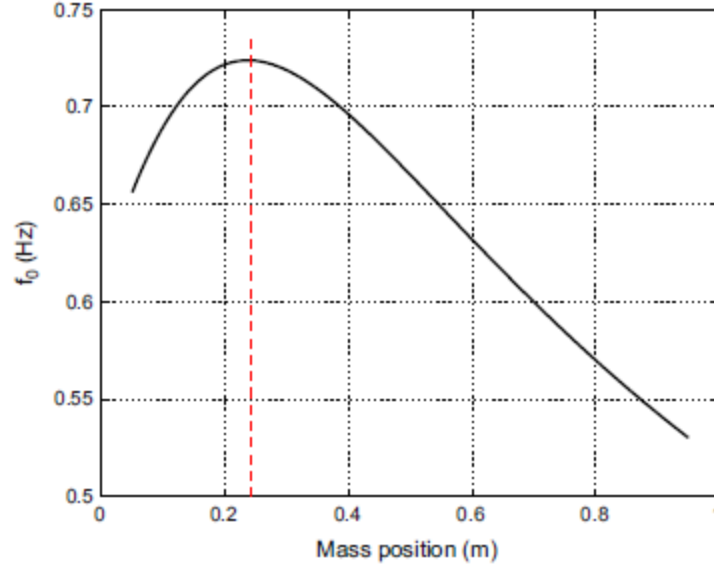


Fig. 7. Representation of the frequency  $f_0$  as a function of  $s$ . The function has a maximum at about  $s = 0.237$  m.

This function has a maximum at about  $s = 0.237$  m so that there are values of frequency that can be associated to two different mass positions. This might lead to extra difficulties in interpreting the results.

#### 4. Flexural vibrations

In this section, the flexural vibrations of the pendulum are considered. First of all, the theoretical model representing the flexural motion of the structure under study is presented; successively the unknown physical parameters are estimated and a procedure based on the Rayleigh-Ritz method is applied to extract the analytical “frozen” frequencies. Finally, these frequencies are compared with those obtained by the ST-SSI method.

##### 4.1. Beam model with no added mass

The pendulum, in the transversal plane, can be considered as an Euler-Bernoulli beam with a rotational spring with stiffness  $K$ , to take into account the fact that the clamping

condition is not perfect.

The effective beam length cannot be considered equal to  $L_b = 1$  m because there is a metallic plate, with a length equal to  $b_p = 0.063$  m, that limits the flexural vibrations of the pendulum (see Fig. 2). Moreover, as done in [28] for cables of a bridge, it is generally useful to consider an equivalent length  $L_{eq}$  corresponding to the identified natural frequencies and to the other parameters of the system. The representation of the model is proposed in Fig. 8. This is valid only for the flexural motion, because the metallic plate does not influence the swings in the other plane (apart from its added inertia).

The general mode shape of the beam is of the form

$$\phi(x) = A \cos(\alpha x) + B \sin(\alpha x) + C \cosh(\alpha x) + D \sinh(\alpha x) \quad (11)$$

where  $\alpha^4 = \mu \omega^2 / EI$  and the boundary conditions are the following:

$$\phi(0) = 0 \quad \phi''(0) = \frac{K}{EI} \phi'(0) \quad (12a)$$

$$\phi''(L_{eq}) = 0 \quad \phi'''(L_{eq}) = 0 \quad (12b)$$

#### 4.2. Estimation of unknown parameters

In addition to the unknown equivalent length, the clamping condition is not known as often happens in real applications, and the area moment of inertia of the beam is difficult to be estimated because of its complex geometry (see Fig. 1). Then, three physical parameters are considered as unknowns:

- $L_{eq}$ : equivalent length of the beam
- $k$ : normalized rotational stiffness of the beam
- $EI$ : bending stiffness of the beam

The parameter  $k$  is usually considered in these cases instead of  $K$  [29], because it gives an idea of the “degree of clamping”. With this coefficient, it is possible to consider all the intermediate configurations between the simply support case ( $k = 0$ ) and the perfect clamp case ( $k = 1$ ). The relationship between  $K$  and  $k$  is:

$$\frac{K}{EI} = \frac{1}{L_{eq}} \frac{\pi^4 k}{(1-k)} \quad (13)$$

The natural frequencies are obtained by means of the following formula:

$$f_r = \frac{z_r^2}{2\pi} \sqrt{\frac{EI}{\mu}} \quad (14)$$

where  $z_r$  are the zeros of the determinant of the matrix defined by imposing the conditions expressed by Eq. (12) to the mode shapes of Eq. (11), and  $\mu$  is the mass per unit of length of the beam.

Now, let us consider an experimental test in which the pendulum is not swinging and there are no added masses on it. In this configuration, the pendulum can be considered as the beam described in this chapter.

Considering that the clamp is not perfect, the equivalent length  $L_{eq}$  has been taken equal to 0.85 m. In order to estimate  $k$  and  $EI$ , a double iteration has been applied on different values of the physical unknowns. The best values are chosen as those minimizing the difference with the first three natural frequencies identified with the classical subspace methods [7]. The optimization procedure leads to the following parameters:

$$k = 0.07, \quad EI = 20.5 \text{ N}\cdot\text{m}^2 \quad (15)$$

In Table 3 the identified frequencies are listed together with the frequencies calculated with the optimal values.

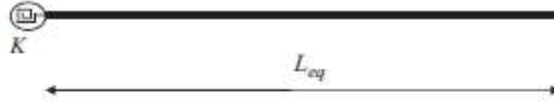


Fig. 8. The beam model under analysis.

**Table 3**

First three flexural frequencies of the pendulum, no added mass.

Identified frequencies	Reconstructed frequencies
$f_1 = 5.25 \text{ Hz}$	$f_1 = 5.24 \text{ Hz}$
$f_2 = 34.91 \text{ Hz}$	$f_2 = 34.99 \text{ Hz}$
$f_3 = 102.90 \text{ Hz}$	$f_3 = 101.37 \text{ Hz}$

#### 4.3. Identification of the flexural frequencies

The ST-SSI method has been used for the identification of the natural frequencies in the case of load moving on the pendulum, because the system is time-varying. They are extracted by considering the signals recorded by the four monoaxial accelerometers introduced in Section 3.1.1.

By referring to Eq. (2), the output signals  $y$  correspond to the four recorded accelerations, while  $u = 0$ , meaning that no inputs have been applied. About the identification, the signals have been decimated with a factor of 10. Moreover, 80 samples are considered in each window, corresponding to a time duration of 3.125 s, with an overlap of 79 samples. With these parameters, each window included from 8 to 15 periods of the first natural frequency. The identified frequencies are successively compared with those obtained by the Rayleigh-Ritz method, a well known approach in the field of dynamics [30]. All the analytical developments are presented in Appendix B.

Two cases, among the several created in the laboratory, are represented. They are named:

- 01: the mass is moving upward
- 02: the mass is moving at first downward and successively upward

In Figs. 9a and 9b, the signals of the linear potentiometer are shown for cases 01 and 02. In particular, the positions of the mass are depicted by inverting the axis scale, in order to agree with the direction of  $s(t)$  in Fig 3.

In Fig. 9c (case 01), the identified frequency is increasing while in Fig. 9d (case 02) the frequency is initially decreasing and then increasing. The estimations follow the corresponding trends of the mass positions. They are very clear and it is possible to note that the range of variation of the frequency is very large: this is due to the heavy travelling load, its mass being almost twice the mass of the beam.

The identified frequency can be displayed as a function of the mass position on the pendulum. In this way, both cases show the same trend, as can be seen in Fig. 10. The frequencies are compared with the theoretical curve obtained with the Rayleigh-Ritz method. The difference among this curve and the identified frequencies is quite small, and the error is mainly due to a couple of reasons:

- the Rayleigh-Ritz method does not take into account the dynamic effect due to the relative velocity  $\dot{s}$  of the travelling mass.
- the physical parameters linked to the mass, e.g. the moment of inertia  $I_d$ , can be slightly different from the nominal values.

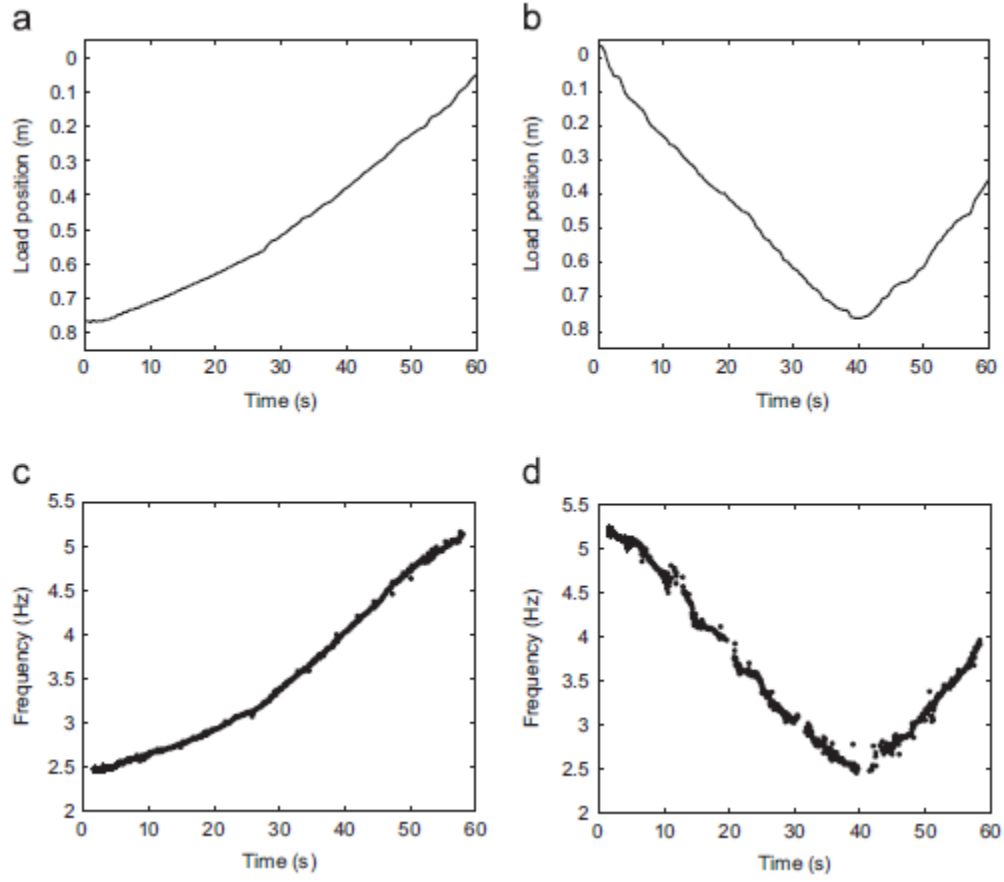


**Fig. 9.** Positions of the mass and corresponding identified first flexural frequency, for two different cases: (a)-(c) case 01; (b)-(d) case 02.

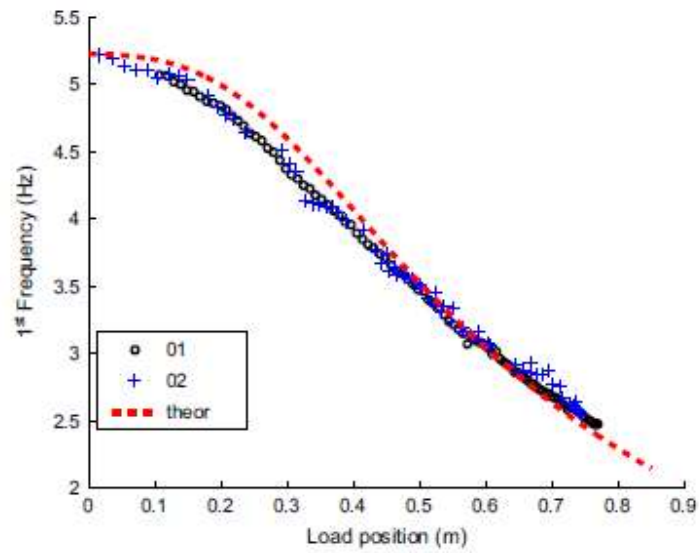


**Fig. 10.** Flexural vibrations: comparison among the identified frequencies (ST-SSI) of two experimental cases (01 and 02) and the theoretical curve obtained with the Rayleigh-Ritz method



## 5. Motion of the pendulum

The swinging motion has been analysed by applying the NSI and the ST-SSI methods separately. This is due to the main drawback affecting them when studying such a time-variant *and* nonlinear system: both methods cannot distinguish the time-variant contribution from the nonlinear one, since the effect of both contributions consists of swinging frequency variations.

As a consequence, the study of the swinging motion has been divided into two parts. In the first one, dedicated to the fixed mass case, the NSI method is used to identify the nonlinear contribution and the “underlying” linear frequency: to validate the method, the results are compared with the known actual values. Then, the system parameters are updated to build a new NSI-based model. In the second part, which focuses on the swings in presence of a moving mass, the ST-SSI method is applied: as a reference, the baseline frequencies described in Section 3.2.2 are computed by using the previously updated parameters, so that all information given in Table 2 is no more needed (except for the value  $m_m$  of the travelling mass).

### 5.1. Fixed mass: the NSI method

In this section, the NSI method is applied in order to identify the system parameters as only depending upon the nonlinear effects due to the large swings. To this aim, the travelling mass has been fixed along the beam in two different positions, namely  $\bar{s} = 0.91$  m and  $\bar{s} = 0.5$  m, so that the starting point is Eq. (7). Moreover, in order to apply the NSI method, it is useful to consider the Taylor expansion of the sine (for  $\theta \cong 0$ ):

$$\sin \theta \cong \theta - \frac{1}{6} \theta^3 + K + \frac{(-1)^n}{(2n+1)!} \theta^{2n+1} + o(\theta^{2n+2}) \quad (16)$$

By truncating the expansion in Eq. (16) to  $n = 2$  (for this value the level of accuracy is excellent, when  $|\theta| < \pi/2$ ), Eq. (7) can be written as:

$$\bar{I}_{tot}\ddot{\theta}(t) + c_v\dot{\theta}(t) + \bar{P}_{tot}(\theta(t) + \beta_1\theta(t)^3 + \beta_2\theta(t)^5) = 0 \quad (17)$$

where  $\beta_j = \frac{(-1)^j}{(2j+1)!}$  for  $j = 1, 2$  are the coefficients of the nonlinear terms in the Taylor expansion. In this way, the linear part of the equation and the nonlinear feedback force can be separated as seen in Section 2.2:

$$\bar{I}_{tot}\ddot{\theta}(t) + c_v\dot{\theta}(t) + \bar{P}_{tot}\theta(t) = -\beta_1\bar{P}_{tot}\theta(t)^3 - \beta_2\bar{P}_{tot}\theta(t)^5 \quad (18)$$

From Eq. (18), the discrete state-space model defined in Section 2.2 can be identified by means of subspace methods [7], by only using the system output vector  $y = \theta(t)$  measured by the rotary sensor described in Section 3.1.1 and the input (feedback forces)  $u = \begin{bmatrix} -\theta(t)^3 & -\theta(t)^5 \end{bmatrix}^T$ . The natural frequency of the “underlying” linear system (i.e. linear part of the equation of motion) can be extracted by calculating the eigenvalues of the identified matrix  $A$ : in the case of a pendulum, the linear frequency sought for is equal to the frequency  $f_0$  of “small” swings.

The identification of the nonlinear coefficients should be carried on as follows, by exploiting the method used in [17] and the particular form of the nonlinear coefficients defined through Eqs. (16) and (17). In fact, they are defined as  $\mu_j = \beta_j \bar{P}_{tot}$  for  $j = 1, 2$ , so they are both dependent on  $\bar{P}_{tot}$ . Eq. (4) turns into  $H_E(\omega) = \begin{bmatrix} H\mu_1 & H\mu_2 \end{bmatrix}$ , where  $H(\omega)$  is the FRF of the “underlying” linear system.

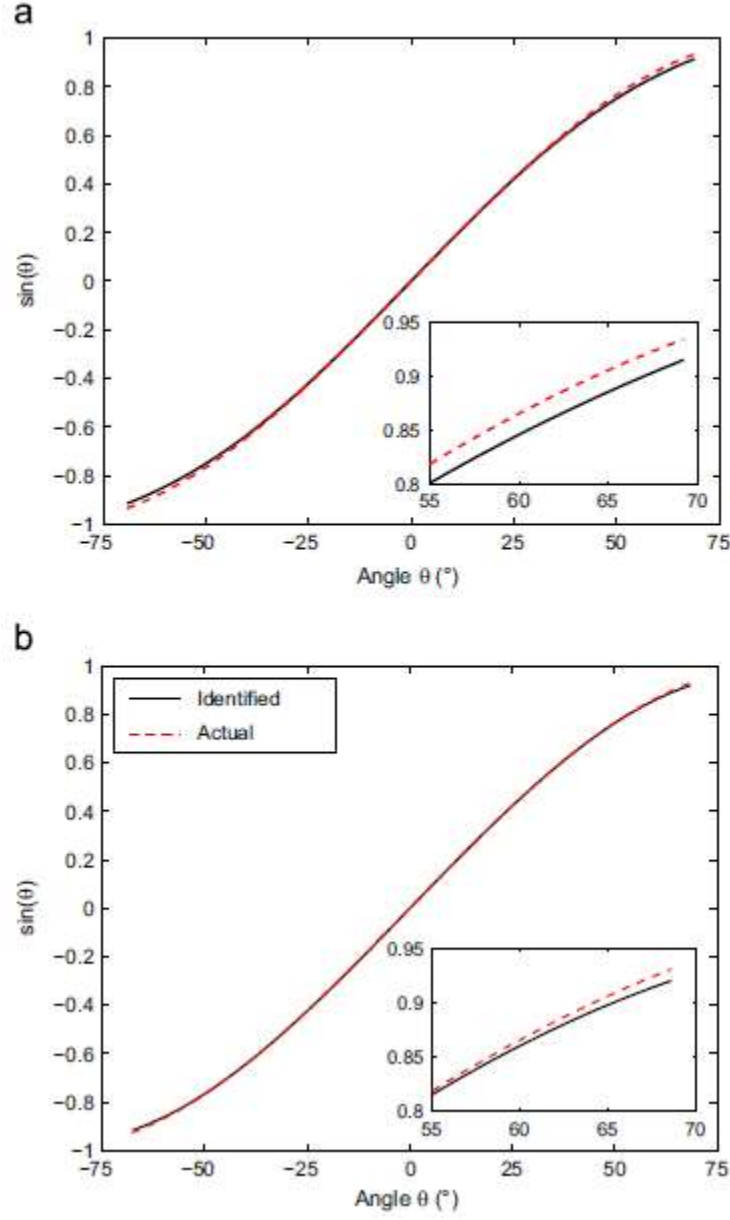


**Fig. 11.** Estimates of the sinusoidal term. (a)  $\bar{s} = 0.91$  m. (b)  $\bar{s} = 0.5$  m. The actual value  $\sin\theta$  is represented with a dashed line. A magnification for large amplitudes is also shown.

In particular, when  $\omega = 0$  then  $H(0) = \bar{P}_{tot}^{-1}$  and an estimate of the coefficients defining the Taylor expansion of the sine in Eq. (16) can be obtained as

$$H_E(\omega = 0) = [\beta_1 \quad \beta_2]. \quad (19)$$

The NSI method as described above has been repeatedly applied to several time records where the nonlinear contribution was more important.  $N$  overlapping time windows of 30 seconds each, covering a range of decreasing amplitudes from 70 to 45 degrees, have been selected: in particular,  $N = 20$  for the case  $\bar{s} = 0.91$  m and  $N = 11$  for  $\bar{s} = 0.5$  m, since for the latter the range of amplitudes is swept faster. The results are presented hereafter.

The nonlinear terms are reconstructed by using the Taylor expansion in Eq. (16) of the sine, with the estimated values  $\beta_1$  and  $\beta_2$  obtained through Eq. (19). Fig. 11 shows a comparison between the actual value of  $\sin\theta$  and the estimated Taylor expansion, for the first window (i.e. largest amplitudes). Note that similar results, in terms of accuracy, are obtained for each of the windows used. In Fig. 11a the case  $\bar{s} = 0.91$  m is presented: good agreement can be seen, with an error of 2% in correspondence with the maximum value of  $\theta$ . In Fig. 11b the case  $\bar{s} = 0.5$  m is presented: excellent agreement can be seen, with an error of 1%.

In Fig. 12 the identified natural frequencies of the “underlying” linear system with fixed mass in  $\bar{s} = 0.91$  m (Fig. 12a) and  $\bar{s} = 0.5$  m (Fig. 12b) are shown. For each window, an estimate of the frequency is obtained (represented by a circle) and a comparison with the expected value  $f_0$  (the red dashed line), computed from the nominal values in Table 2, is also given.

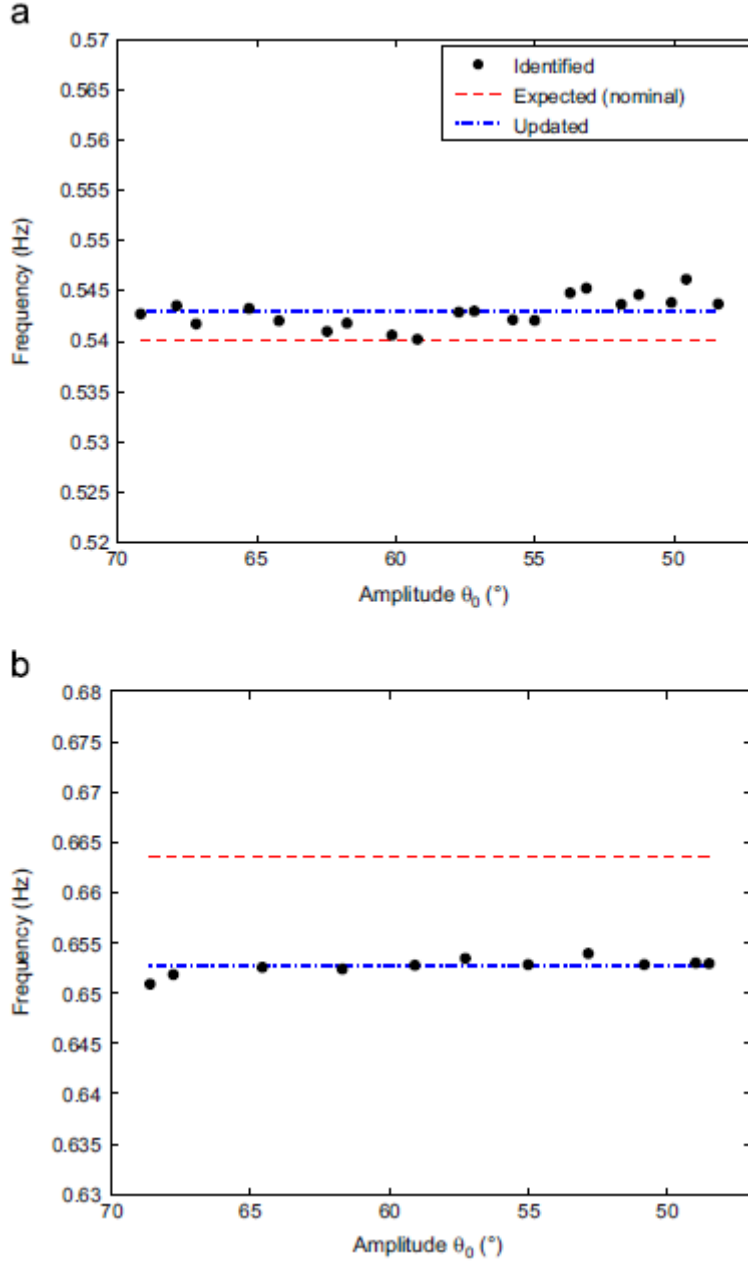


**Fig. 12.** Estimates of the frequency of oscillations (represented by circles). (a)  $\bar{s} = 0.91$  m. (b)  $\bar{s} = 0.5$  m. The “expected” (nominal) value  $f_0$  is represented with a red dashed line. The updated value  $f_{0,up}$  is represented with a blue dash-dotted line

The identified values are placed along a constant line, thus validating the removal of the nonlinear contribution carried out by the NSI method, but a bias can be observed

(especially in Fig. 12b). This is caused by inaccuracies in the characteristics of the components or by the presence of instrumentation (accelerometers, cables). An updating procedure is then performed, in order to build a new model (the blue dash-dotted line on Fig. 12) based on identified results. In more detail, consider Eq. (10), which defines the swinging frequency for small amplitudes, and assume that the values of  $I$  and  $P$  have to be updated to fit the identified model. In the identification step, the NSI estimates  $\hat{f}_{0,j} = \hat{f}_0(\bar{s}_j)$  for two fixed mass positions  $\bar{s}_1 = 0.91$  m and  $\bar{s}_2 = 0.5$  m have been obtained: in order to have a single value for each position, the mean value over the  $N$  identified estimates is computed. By assuming that the moving mass  $m_m = 0.5025$  kg is also known, the following system of equations can be obtained from Eq. (10), in the new unknowns  $I_{up}$  and  $P_{up}$ :

$$\begin{bmatrix} -(2\pi\hat{f}_{0,1})^2 & 1 \\ -(2\pi\hat{f}_{0,2})^2 & 1 \end{bmatrix} \begin{Bmatrix} I_{up} \\ P_{up} \end{Bmatrix} = \begin{Bmatrix} (2\pi\hat{f}_{0,1})^2 m_m \bar{s}_1^2 - g m_m \bar{s}_1 \\ (2\pi\hat{f}_{0,2})^2 m_m \bar{s}_2^2 - g m_m \bar{s}_2 \end{Bmatrix}. \quad (20)$$

A comparison between the nominal and the updated values is given in Table 4: as expected, the updated quantities are higher because of the influence of instrumentation.

**Table 4**Comparison between nominal and updated  $I$  and  $P$ .

	$I$ (kg m <sup>2</sup> )	$P$ (kg m <sup>2</sup> s <sup>-2</sup> )
Nominal	0.0973	1.4294
Updated	0.1292	1.8380
$\Delta$ =Updated-Nominal	$\Delta I = 0.0319$	$\Delta P = 0.4086$

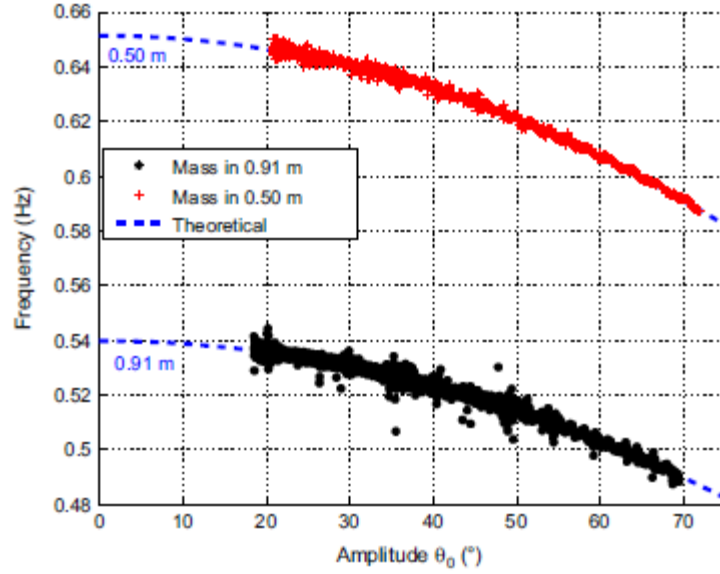


**Fig. 13.** Comparison of two cases with fixed mass on the pendulum (in 0.91 m and 0.50 m respectively) with the theoretical frequencies calculated on the same mass position.

As a further control, the contributions  $I_{acc}$  and  $P_{acc}$  due to the accelerometers can be evaluated by considering the information given in Table 1:

$$I_{acc} = m_{tri} s_{tri}^2 + m_{mono} \sum_{j=1}^4 s_{mono,j}^2 = 0.0295 \text{ kg m}^2 \quad (21a)$$

$$P_{acc} = g \left( m_{tri} s_{tri} + m_{mono} \sum_{j=1}^4 s_{mono,j} \right) = 0.3327 \text{ kg m}^2 \text{ s}^{-2} \quad (21b)$$

These quantities are in good agreement with  $\Delta I$  and  $\Delta P$  shown in Table 4, this highlighting the contribution of the accelerometers in the dynamics of the pendulum.

In order to validate the updated model, a first step consists of computing the new values of the “expected” swinging frequency for both the cases  $\bar{s} = 0.91$  m and  $\bar{s} = 0.5$  m. It is called updated frequency and it is defined through Eq. (10) as

$$f_{0,up}(\bar{s}) = \frac{1}{2\pi} \sqrt{\frac{(P_{up} + m_m g \bar{s})}{(I_{up} + m_m \bar{s}^2)}}. \quad (22)$$

In Fig. 12 the updated frequency (the blue dash-dotted line) and the NSI estimates are compared: an excellent agreement can be observed, confirming the accuracy of the identified model.

In this way, by parameter identification (for the nonlinear terms) and updating (for the linear terms) a general model representing the experimental pendulum with fixed mass is defined:

$$(I_{up} + m_m \bar{s}^2) \ddot{\theta}(t) + c_v \dot{\theta}(t) + (P_{up} + m_m g \bar{s})(\theta + \beta_1 \theta^3 + \beta_2 \theta^5) = 0 \quad (23)$$

At this point, all information given in Table 2 is no more needed (except for the value  $m_m$  of the travelling mass): the updated parameters  $I_{up}$  and  $P_{up}$  can be used to compute the baseline frequencies of Eqs. (9) and (10), as a reference for the application of ST-SSI.

#### 5.1.1. Estimation of the frequencies with ST-SSI

To identify the swinging frequencies the ST-SSI method is finally applied to the angular position signal. In this case, the identified values can be depicted as a function of the amplitude  $\theta_0$  and compared with the baseline frequencies described in Section 3.2.2. The results are plotted in Fig. 13, where the theoretical curves have been calculated for two different positions of the mass (0.50 m and 0.91 m), for different angular amplitudes.



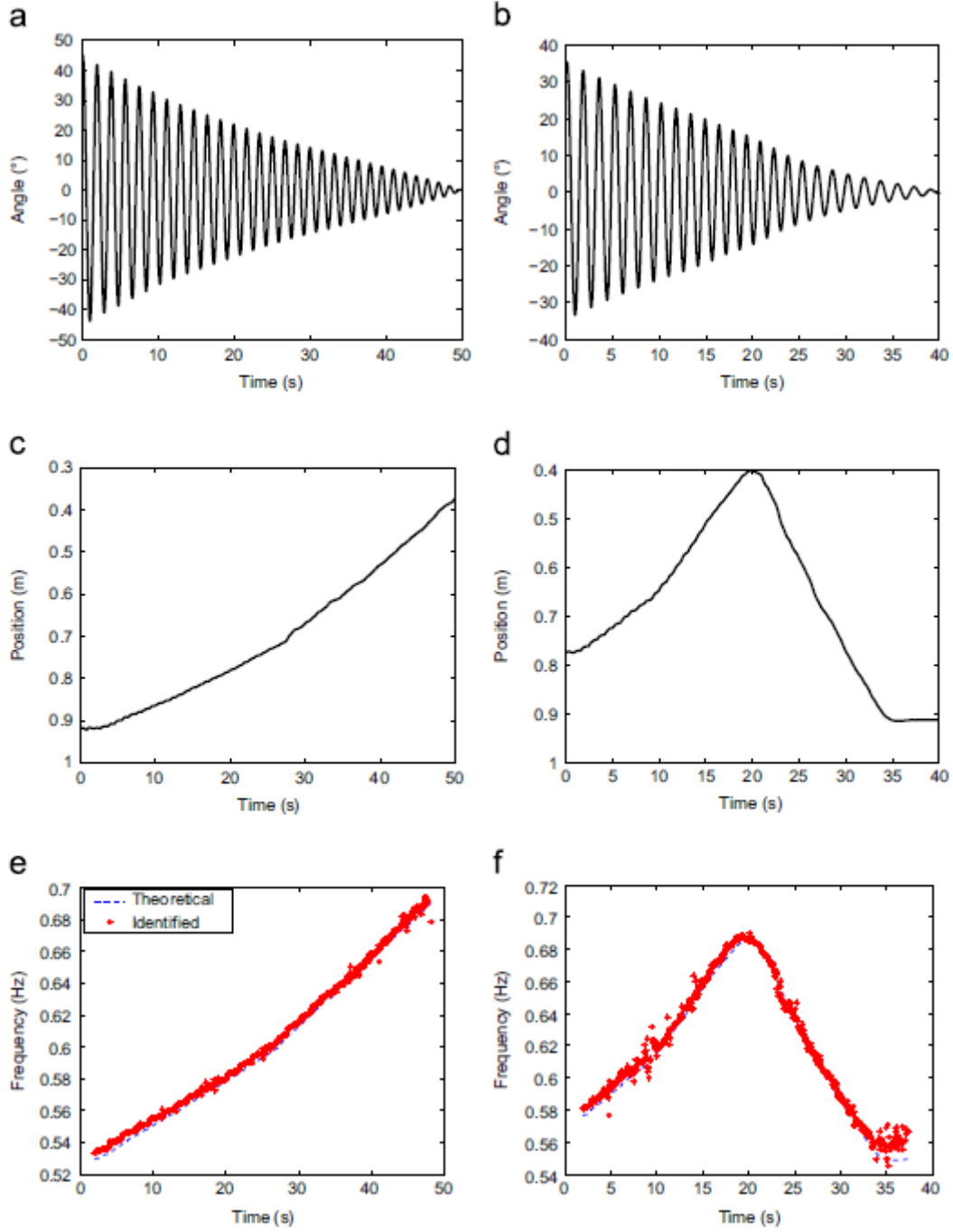


**Fig. 14.** Nonlinear oscillations for cases M1 (a-c-e) and M2 (b-d-f): time evolution of the oscillation angle (a-b), of the mass position (c-d) and frequencies calculated with ST-SSI, compared with the theoretical ones (e-f).

The ST-SSI identification is applied on signals decimated with a factor of 12. 60 samples are considered in each window, corresponding to a time duration of 2.81 s, with an overlap

of 59 samples. With these parameters, each window included from 1.5 to 2 periods of the first natural frequency.

The identified and theoretical frequencies of the nonlinear pendulum are very close, confirming that the adopted model is able to predict the evolution of the frequencies, in the case of swings with a fixed mass on the pendulum.

## 5.2. Moving mass: the ST-SSI method

Let us consider two cases, in which the load is travelling on the pendulum, this producing both nonlinear and time-varying effects:

- case M1: the mass is moving upward
- case M2: the mass is moving firstly upward and then downward

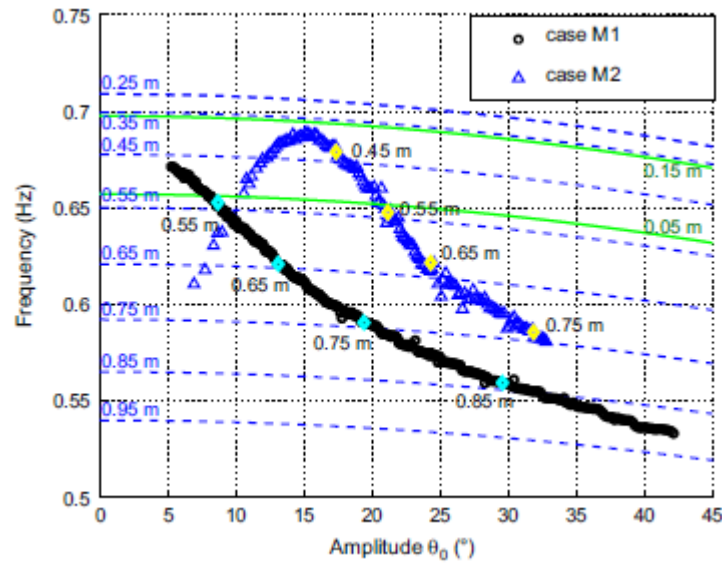


**Fig. 15.** Nonlinear oscillations: comparison among the frequencies of the experimental cases M1/M2 and the baseline frequencies built for ten different load positions. The diamonds on the experimental curves highlight specific mass positions, measured by the linear potentiometer.

For both cases, the time histories of the angle and the load position are shown in Fig. 14, together with the frequencies identified by means of the ST-SSI method and compared to

those obtained by applying Eqs. (9) and (10) with the updated parameters  $I_{up}$  and  $P_{up}$ .

In order to have a final visualization, Fig. 15 shows the identified frequencies and compares them with the baseline frequencies  $\bar{f}$  introduced in Section 3.2. Ten different mass positions on the pendulum (from 0.05 m to 0.95 m) have been plotted to verify the correspondence among frequency, angle amplitude and mass position (in a certain time instant) for the theoretical and the identified models. Some mass positions measured by the linear potentiometer have been marked on the graph by means of diamonds, both for the case M1 and the case M2. The identified values are very close to the predicted frequencies, for both the experiments.

## 6. Conclusions

The paper is focused on the experimental study of a time-varying inertia pendulum; for large swinging amplitudes its equation of motion must definitely include the nonlinear terms. It hence becomes a nonlinear time-varying system which is analysed through the application of two techniques for the identification of linear time-varying systems (ST-SSI) and nonlinear systems with constant coefficients (NSI).

The flexural motion is studied by proposing a model of a beam travelled by a moving load, while the nonlinear equation of the swinging motion is inspected in order to obtain the theoretical (baseline) frequency as depending on the amplitude of swings and on the load position. These models are built for comparing the theoretical results with the outcome of the identification procedures herewith developed.

In particular, when studying the flexural motion only the ST-SSI method has been applied, since the system is linear time-variant. Both the NSI and the ST-SSI methods have been

applied in studying the swinging motion, as follows: (1) with fixed mass, the NSI method is used to identify the nonlinear contribution and the “underlying” linear frequency: to validate the method, the results are compared with the known actual values; (2) the frequency is adopted to update the system parameters and to build a new model; (3) the updated parameters are used to compute the baseline frequencies, as a reference for the application of ST-SSI.

The paper demonstrates that a good agreement between the predicted and the identified frequencies can be achieved, for the entire domain of possible configurations, in terms of swinging amplitude and mass position. The paper is also one of the first studies for such a kind of nonlinear and variable mass system, which has not been fully treated in literature yet; in this sense, it opens new scenarios to a number of further investigations, including a closer interaction between nonlinear and time variant behaviour, and the role of the speed of the travelling mass.

## **Appendix A: swinging frequency of the undamped pendulum**

In the following, the behaviour of the undamped pendulum in case of large swings is studied, with fixed mass, in order to achieve an analytical expression of its time-varying frequency [22]. The starting point is Eq. (7), with the assumption that  $c_v = 0$ .

Consider the energy balance for the undamped pendulum (the time dependency is omitted from now on), in which  $\theta_0$  stands for the maximum amplitude (note that  $\dot{\theta} = 0$  in  $\theta_0$ ):

$$\frac{1}{2} \bar{I}_{tot} \dot{\theta}^2 + \bar{P}_{tot} (1 - \cos \theta) = \bar{P}_{tot} (1 - \cos \theta_0) \quad (\text{A.1a})$$

By using the trigonometric identity  $\cos \theta = 1 - 2 \sin^2(\theta/2)$ , we obtain

$$\frac{1}{2}\bar{I}_{tot}\dot{\theta}^2 = 2\bar{P}_{tot}\left(\sin^2 \frac{\theta_0}{2} - \sin^2 \frac{\theta}{2}\right) \quad (\text{A.1b})$$

and then

$$dt = \frac{1}{2} \sqrt{\frac{\bar{I}_{tot}}{\bar{P}_{tot}}} \left( \sin^2 \frac{\theta_0}{2} - \sin^2 \frac{\theta}{2} \right)^{-\frac{1}{2}} d\theta \quad (\text{A.2})$$

By integrating both sides of Eq. (A.2) between 0 and  $\theta_0$ , a quarter of the period  $T$  is

obtained on the left and then:

$$T = 2 \sqrt{\frac{\bar{I}_{tot}}{\bar{P}_{tot}}} \int_0^{\theta_0} \left( \sin^2 \frac{\theta_0}{2} - \sin^2 \frac{\theta}{2} \right)^{-\frac{1}{2}} d\theta \quad (\text{A.3})$$

We can now apply the following relations (note that  $T_0$  is the period for “small” swings)

$$T_0 = 2\pi \sqrt{\frac{\bar{I}_{tot}}{\bar{P}_{tot}}}, \quad \sin \phi = \frac{\sin(\theta/2)}{\sin(\theta_0/2)} \quad (\text{A.4})$$

to rewrite Eq. (A.3) as

$$T = \frac{2}{\pi} T_0 K(k) \quad (\text{A.5})$$

where  $k = \sin(\theta_0/2)$  and

$$K(k) = \int_0^{\pi/2} \frac{d\phi}{\sqrt{1 - k^2 \sin^2 \phi}}, \quad \text{for } |k| < 1 \quad \text{and} \quad |\theta_0| < \pi \quad (\text{A.6})$$

is the incomplete elliptic integral of the first kind. This integral can be approximated, for example, by expanding the integrand function in power series or by using an accurate arithmetic-geometric mean [23]. The analytical expression of the swinging frequency is obtained by simply inverting Eq. (A.5).

## Appendix B: application of the Rayleigh-Ritz method

The Rayleigh-Ritz method has been applied on the model considered in Section 4.3.

The contributions of potential energy are due to the bending stiffness of the beam and to the rotational spring:

$$U_{EI}(t) = \frac{1}{2} \int_0^{L_{eq}} EI \left( \frac{\partial^2 v(x,t)}{\partial x^2} \right)^2 dx \quad (\text{B.1a})$$

$$U_K(t) = \frac{1}{2} K \left( \frac{\partial v(x,t)}{\partial x} \right)^2 \Big|_{x=0} \quad (\text{B.1b})$$

where  $v(x,t)$  is the transverse displacement of the beam.

The terms related to the kinetic energy are linked to the mass per unit of length of the beam, to the mass and moment of inertia of the moving load, respectively.

$$T_\mu(t) = \frac{1}{2} \int_0^{L_{eq}} \mu \left( \frac{\partial v(x,t)}{\partial t} \right)^2 dx \quad (\text{B.1c})$$

$$T_m(t) = \frac{1}{2} m \left( \frac{\partial v(x,t)}{\partial t} \right)^2 \Big|_{x=\bar{s}} \quad (\text{B.1d})$$

$$T_I(t) = \frac{1}{2} I_d \left( \frac{\partial^2 v(x,t)}{\partial x \partial t} \right)^2 \Big|_{x=\bar{s}} \quad (\text{B.1e})$$

where  $\bar{s}$  is the load position along the beam.

According to the Rayleigh-Ritz method, an approximate solution of the eigenvalue problem can be constructed in the form of the linear combination

$$f(x) = \sum_{i=1}^n a_i \phi_i(x) \quad (\text{B.2})$$

where  $a_i$  are unknown constant coefficients and  $\phi_i(x)$  are trial functions. A good choice

are the polynomials:

$$f(x) = \sum_{i=1}^n a_i x^i \quad (\text{B.3})$$

where  $n$  is the number of polynomial terms. The first two derivatives are:

$$f'(x) = \sum_{i=1}^n a_i i x^{i-1} \quad (\text{B.4a})$$

$$f''(x) = \sum_{i=1}^n a_i i(i-1) x^{i-2} \quad (\text{B.4b})$$

Since the Rayleigh's quotient  $R$  can be written as

$$R = \omega^2 = \frac{U_{\max}}{\tilde{T}} = \frac{U_{EI,\max} + U_{k,\max}}{\tilde{T}_\mu + \tilde{T}_m + \tilde{T}_l} = \frac{Q}{P} \quad (\text{B.5})$$

then the reference equation is

$$\omega^2 = \frac{EI \int_0^{L_{eq}} (f''(x))^2 dx + K(f'(0))^2}{\mu \left[ \int_0^{L_{eq}} f^2(x) dx \right] + mf^2(\bar{s}) + I_d (f'(\bar{s}))^2} = \frac{EIN_1 + KN_2}{\mu D_1 + mD_2 + I_d D_3} \quad (\text{B.6})$$

In the Rayleigh-Ritz method the unknown coefficients  $a_r$  are determined so that the

Rayleigh's quotient is stationary. This is equivalent to

$$\frac{\partial R}{\partial a_i} = \frac{P \frac{\partial Q}{\partial a_i} - Q \frac{\partial P}{\partial a_i}}{P^2} = 0 \quad (\text{B.7})$$

Therefore it is necessary to calculate the derivatives of the numerator  $Q$  and denominator

$P$  with respect to the coefficients and then build the following eigenvalues problem:

$$[\tilde{K}]\{a\} = \Lambda [\tilde{M}]\{a\} \quad (\text{B.8})$$

where  $\Lambda$  collects the squares of the angular frequencies.

Let us analyze each term separately, starting from the numerator, which includes two terms.

$$\begin{aligned}
 N_1 &= \int_0^{L_{eq}} (f''(x))^2 dx = \int_0^{L_{eq}} \left( \sum_{i=1}^n a_i i(i-1) x^{i-2} \right)^2 dx = \\
 &= \sum_{i=1}^n a_i^2 \frac{i^2(i-1)^2}{2i-3} L_{eq}^{2i-3} + \sum_{i=1}^n \sum_{j=1, i \neq j}^n a_i a_j \frac{ij(i-1)(j-1)}{i+j-3} L_{eq}^{i+j-3}
 \end{aligned} \tag{B.9a}$$

$$N_2 = (f'(0))^2 = a_1^2 \tag{B.9b}$$

$$\tilde{K}_{i,j} = 2EI \frac{ij(i-1)(j-1)}{i+j-3} L_{eq}^{i+j-3} \tag{B.9c}$$

In the case  $i = j = 1$ , there is an additional term in Eq. (B.9c) equal to  $2K$ , which comes from Eq. (B.9b).

The denominator includes three terms.

$$\begin{aligned}
 D_1 &= \int_0^{L_{eq}} f^2(x) dx = \int_0^{L_{eq}} \left( \sum_{i=1}^n a_i x^i \right)^2 dx = \\
 &= \sum_{i=1}^n a_i^2 \frac{1}{2i+1} L_{eq}^{2i+1} + \sum_{i=1}^n \sum_{j=1, i \neq j}^n a_i a_j \frac{1}{i+j+1} L_{eq}^{i+j+1}
 \end{aligned} \tag{B.10a}$$

$$D_2 = f^2(\bar{s}) = \sum_{i=1}^n a_i^2 \bar{s}^{2i} + \sum_{i=1}^n \sum_{j=1, i \neq j}^n a_i a_j \bar{s}^{i+j} \tag{B.10b}$$

$$D_3 = (f'(\bar{s}))^2 = \sum_{i=1}^n a_i^2 i^2 \bar{s}^{2i-2} + \sum_{i=1}^n \sum_{j=1, i \neq j}^n a_i a_j ij \bar{s}^{i+j-2} \tag{B.10c}$$

$$\tilde{M}_{i,j} = \mu \tilde{M}_{i,j}^{(1)} + m \tilde{M}_{i,j}^{(2)} + I_d \tilde{M}_{i,j}^{(3)} = \frac{2\mu}{i+j+1} L_{eq}^{i+j+1} + 2m \bar{s}^{i+j} + 2I_d ij \bar{s}^{i+j-2} \tag{B.10d}$$

The frequencies are calculated by applying Eq. (B.8) with Eq. (B.9c) and Eq. (B.10d).

## References

[1] K. Liu, Identification of Linear Time-Varying Systems, Journal of Sound and Vibration 206 (1997), 487-505.



- [2] K. Liu, Extension of Modal Analysis to Linear Time-Varying Systems, *Journal of Sound and Vibration* 226 (1999), 149-167.
- [3] F. Tasker, A. Bosse, S. Fisher, Real-time modal parameters estimation using subspace methods: applications, *Mechanical System and Signal Processing* 12 (6) (1998), 809-823.
- [4] S.-W. Lee, J.-S. Lim, S.J. Baek, K.-M. Sung, Time-varying signal frequency estimation by VFF Kalman filtering, *Signal Processing* 77 (1999), 343-347.
- [5] A.G. Poulimenos, S.D. Fassois, Output-Only Identification of a time-varying structure via functional series TARMA models, *Mechanical Systems and Signal Processing* 23 (2009), 1180-1204.
- [6] A. Bellino, L. Garibaldi, S. Marchesiello, Time-Varying Output-Only Identification of a cracked beam, *Key Engineering Materials* 413-414 (2009), 643-650.
- [7] P. Van Overschee, B. De Moor, *Subspace Identification for Linear Systems: Theory, Implementation, Applications*, Kluwer Academic Publishers, Boston / London / Dordrecht, 1996.
- [8] A. Bellino, L. Garibaldi, S. Marchesiello, Determination of moving load characteristics by output-only identification over the Pescara beams, *Journal of Physics, Conference Series* 305 (2011).
- [9] B. Moaveni, E. Asgarieh, Deterministic-stochastic subspace identification method for identification of nonlinear structures as time-varying linear systems, *Mechanical System and Signal Processing* 31 (2012), 40-55.
- [10] L. Bornn, C.R. Farrar, G. Park, Damage detection in initially nonlinear systems, *International journal of Engineering Science* 48 (2010), 909-20.
- [11] G. Kerschen, K. Worden, A. F. Vakakis, J.-C. Golinval, Past, present and future of

- nonlinear system identification in structural dynamics, *Mechanical Systems and Signal Processing* 20 (2006), 505-592.
- [12] C. M. Richards, R. Singh, Identification of multi-degree-of-freedom non-linear systems under random excitations by the reverse-path spectral method, *Journal of Sound and Vibration* 213 (1998), 673-708.
- [13] S. Marchesiello, Application of conditioned reverse path method, *Mechanical Systems and Signal Processing* 17 (2003), 183-188.
- [14] D. E. Adams, R. J. Allemang, A frequency domain method for estimating the parameters of a non-linear structural dynamic model through feedback, *Mechanical Systems and Signal Processing* 14 (4) (2000), 637-656.
- [15] S. Marchesiello, L. Garibaldi, A time domain approach for identifying nonlinear vibrating structures by subspace methods, *Mechanical Systems and Signal Processing* 22 (2008), 81-101.
- [16] E. Gandino, S. Marchesiello, Identification of a Duffing oscillator under different types of excitation, *Mathematical Problems in Engineering* 2010 (2010), Article ID 695025, 15 pages, doi:10.1155/2010/695025.
- [17] E. Gandino, L. Garibaldi, S. Marchesiello, Pescara benchmarks: nonlinear identification, *Journal of Physics: Conference Series* 305 (2011).
- [18] W. Szyszkowski, E. Sharbati, On the FEM modeling of mechanical systems controlled by relative motion of a member: A pendulum-mass interaction test case, *Finite Elements in Analysis and Design* 45 (2009), 730-742.
- [19] W. Szyszkowski, D.S.D. Stilling, On damping properties of a frictionless physical pendulum with a moving mass, *International Journal of Non-Linear Mechanics* 40 (2005),

669-681.

[20] W. Szyszkowski, D.S.D. Stilling, Controlling angular oscillations through mass reconfiguration: a variable length pendulum case, *International Journal of Non-Linear Mechanics* 37 (2002), 89-99.

[21] A.A. Zevin, L.A. Filonenko, A qualitative investigation of the oscillations of a pendulum with a periodically varying length and a mathematical model of a swing, *Journal of Applied Mathematics and Mechanics* 71 (2007), 892-904.

[22] F.M.S. Lima, P. Arun, An accurate formula for the period of a simple pendulum oscillating beyond the small angle regime, *American Journal of Physics* 74 (2006), 892-895.

[23] C.G. Carvalhes, P. Suppes, Approximations for the period of the simple pendulum based on the arithmetic-geometric mean, *American Journal of Physics* 76 (12) (2008), 1150-1154.

[24] A. Beléndez, E. Arribas, M. Ortuño, S. Gallego, A. Márquez, I. Pascual, Approximate solutions for the nonlinear pendulum equation using a rational harmonic representation, *Computers and Mathematics with Applications*, *in press*.

[25] S. Marchesiello, S. Bedaoui, L. Garibaldi, P. Argoul, Time-dependent identification of a bridge-like structure with crossing loads, *Mechanical System and Signal Processing* 23 (2009), 2019-2028.

[26] L. Garibaldi, S. Marchesiello, E. Bonisoli, Identification and up-dating over the Z24 benchmark, *Mechanical System and Signal Processing* 17 (1) (2003), 153-161.

[27] T. Yokoyama, Vibrations of a hanging Timoshenko beam under gravity, *Journal of Sound and Vibration* 141 (2) (1990), 245-258.

- [28] A. Bellino, S. Marchesiello, A. Fasana, L. Garibaldi, Cable tension estimation by means of vibration response and moving mass technique, *Mécanique et Industries* 11 (2010), 505-512.
- [29] M. A. Ceballos, C.A. Prato, Determination of the axial force on stay cables accounting for their bending stiffness and rotational end restraints by free vibration tests, *Journal of Sound and Vibration* 317 (2008), 127-141.
- [30] A. W. Leissa, The historical bases of the Rayleigh and Ritz methods, *Journal of Sound and Vibration* 287 (2005), 961-978.